Ground-Based Temperature and Humidity Profiling Using Spectral Infrared and Microwave Observations. Part I: Simulated Retrieval Performance in Clear-Sky Conditions

ULRICH LÖHNERT

Institute for Meteorology and Geophysics, University of Cologne, Cologne, Germany

D. D. TURNER

Space Science and Engineering Center, University of Wisconsin—Madison, Madison, Wisconsin

S. CREWELL

Institute for Meteorology and Geophysics, University of Cologne, Cologne, Germany

(Manuscript received 18 June 2008, in final form 13 October 2008)

ABSTRACT

Two independent ground-based passive remote sensing methods are used to retrieve lower-tropospheric temperature and humidity profiles in clear-sky cases. A simulation study for two distinctly different climatic zones is performed to evaluate the accuracies of a standard microwave profiler [humidity and temperature profiler (HATPRO)] and an infrared spectrometer [Atmospheric Emitted Radiance Interferometer (AERI)] by applying a unified optimal estimation scheme to each instrument. Different measurement modes for each instrument are also evaluated in which the retrieval uses different spectral channels and observational view angles. In addition, both instruments have been combined into the same physically consistent retrieval scheme to evaluate the differences between a combined retrieval relative to the single-instrument retrievals. In general, retrievals derived from only infrared measurements yield superior RMS error and bias to retrievals derived only from microwave measurements. The AERI retrievals show high potential, especially for retrieving humidity in the boundary layer, where accuracies are on the order of 0.25–0.5 g m^{-3} for a central European climate. In the lowest 500 m the retrieval accuracies for temperature from elevation-scanning microwave measurements and spectral infrared measurements are very similar (0.2–0.6 K). Above this level the accuracies of the AERI retrieval are significantly more accurate (<1 K RMSE below 4 km). The inclusion of microwave measurements to the spectral infrared measurements within a unified physical retrieval scheme only results in improvements in the high-humidity tropical climate. However, relative to the HATPRO retrieval, the accuracy of the AERI retrieval is more sensitive to changes in the measurement uncertainty. The discussed results are drawn from a subset of ''pristine'' clear-sky cases: in the general case in which clouds and aerosols are present, the combined HATPRO–AERI retrieval algorithm is expected to yield much more beneficial results.

1. Introduction

High-temporal-resolution vertical profiles of atmospheric temperature and humidity are needed by many applications in atmospheric sciences, such as weather forecasting initialization, model evaluation, and process studies. Atmospheric stability in particular is described by the basic meteorological quantities, namely, temperature and humidity profiles. Even today, radiosondes continue to provide a benchmark measurement for determining high-resolution vertical profiles of pressure, temperature, humidity, and wind because all of the parameters can be simultaneously determined and the accuracy is acceptable for a number of meteorological and aerological applications. Operational radiosonde soundings, however, typically provide 12-hourly observations, a temporal resolution that is often not sufficient

Corresponding author address: Dr. Ulrich Löhnert, Institute for Meteorology and Geophysics, Zülpicher Straße 49a, 50674 Köln, Germany.
E-mail: loehnert@meteo.uni-koeln.de

DOI: 10.1175/2008JAMC2060.1

for many meteorological applications, such as resolving boundary layer (BL) transitions or frontal passages. Also a radiosonde ascent drifts with the wind, which can lead to a significant horizontal displacement, and the ascent as such will take ~1 h to profile the troposphere, both of these factors leading to a sampling error. Additionally, many radiosonde sensors show a ''dry bias'' behavior during the daytime (e.g., Cady-Pereira et al. 2008; Turner et al. 2003), an error that is difficult to account for because of its dependence on multiple environmental factors.

Remote sensing methods have the advantage of being able to derive profile information of temperature and humidity with a high temporal resolution but suffer some drawbacks in vertical resolution and accuracy. This paper compares the performance of ground-based temperature and humidity profiling methods in two different spectral regions: microwave and infrared. Using identical retrieval approaches, we will address the following questions: What are the respective merits of microwave and infrared ground-based temperature and humidity profiling, and what can be gained from a combination of both? This study (part I of a planned series) focuses purely on simulations of clear-sky (CS) conditions. The application to measured data will follow in part II, where we are currently analyzing the humidity and temperature profiler–Atmospheric Emitted Radiance Interferometer (HATPRO–AERI) retrieval performance during a field experiment conducted in the Black Forest during the summer of 2007 (Wulfmeyer et al. 2008). The overall goal is to analyze retrieval performance in detail to pursue simultaneous temperature, humidity, and cloud microphysical parameter retrieval in the near future.

Passive microwave radiometry uses frequency bands around the water vapor absorption line at 22.235 GHz for water vapor profiling and around the 60-GHz oxygen complex for temperature profiling. Studies have shown that approximately four to five independent levels of temperature information may be obtained, whereas the number of independent water vapor levels is on the order of two (Löhnert et al. 2008; Hewison 2007). If elevation-scanning measurements are additionally considered, temperature accuracies are within 0.5 K close to the ground and degrade with height to ~1–2 K in the lower troposphere (Crewell and Löhnert 2007), whereas humidity accuracies range on the order of ~0.8 g m^{-3}. These values are more or less independent of the occurrence of clouds, except in cases of heavy precipitation where saturation effects may occur or the instrument is influenced by rainwater on the radome.

Previous studies have shown that multispectral measurements in the infrared contain information on the tropospheric temperature and humidity profile (Smith et al. 1999; Feltz et al. 2003). This information is generally limited to clear-sky cases and cases where clouds are optically thin. However, in the case of an optically thick cloud, information on temperature and humidity may still be obtained below the cloud if the cloud emissivity and temperature are known or retrieved.

In the following, we describe the parallel development of microwave (MW) and infrared (IR) techniques for temperature and humidity retrieval for clear-sky cases using the same optimal estimation retrieval framework for each. These retrieval algorithms are applied to a typical central European climate and a humid tropical climate to be able to interpret the results as a function of vertically integrated water vapor (IWV) amount.

Our goal is to analyze the error characteristics of both approaches and to combine both measurements to evaluate the accuracy that is obtained in a joint retrieval algorithm. The results shown in this study are based purely on virtual measurements derived from radiative transfer simulations to facilitate the retrieval error analysis. In this way we can exclude sources of bias error as a result of erroneous calibration and absorption model uncertainties—errors that are difficult to quantify in general. We underline that the results shown in this paper are only to be interpreted under these circumstances.

The characteristics of the microwave and infrared instruments used for simulation are described in section 2 of this paper, whereas the retrieval framework, which consists of an optimal estimation approach, is described in section 3. In section 4, we evaluate the accuracies of the retrieval procedures, whereby the MW and IR techniques are separately applied to the same cases and compared to each other. We examine the benefits of combining MW and IR approaches in one joint retrieval and also evaluate the impact of using different IR bands and microwave measurement approaches (zenith-only measurements versus zenith-plus-elevation–scanning measurements). In section 5 we provide a summary and an outlook toward describing the cloudy atmosphere with the expected powerful combination of microwave and infrared bands.

2. Instrumentation and simulation

This study employs simulations of two state-of-the-art passive ground-based remote sensing instruments: the microwave profiler HATPRO and the infrared interferometer AERI. In the following, the basic principles and characteristics of each instrument are briefly specified. We also describe the generation of the simulated measurements, illustrating how the instrument characteristics are maintained.

a. HATPRO

The microwave profiler HATPRO was designed as a network-suitable low-cost microwave radiometer that can observe liquid water path (LWP), humidity, and temperature profiles with high temporal resolution up to 1 s (Rose et al. 2005). HATPRO consists of total-power radiometers utilizing direct detection receivers within two bands, M1 and M2 (see Table 1, Fig. 1). The seven channels of band M1 contain information about the vertical profile of humidity through the pressure broadening of the optically thin 22.235-GHz H_2O line and also contain information for determining LWP. The seven channels of band M2 contain information on the vertical profile of temperature resulting from the homogeneous mixing of O_2 throughout the atmosphere. At the opaque center of the O_2 absorption complex at 60 GHz, most of the information originates from near the surface, whereas further away from the line, the atmosphere becomes less and less opaque so that more and more information also originates from higher atmospheric layers.

In addition to the spectral information, angular information can enhance the accuracy of the temperature profile in the boundary layer (Crewell and Löhnert 2007) when the atmosphere in the direct horizontal vicinity (~3 km) of the microwave profiler is assumed to be horizontally homogeneous. Only the brightness temperature from the optically thick frequency bands close to 60 GHz are used in these elevation scans. Because the brightness temperatures vary only slightly with elevation angle, the method requires a highly sensitive radiometer (i.e., low random noise levels), which is typically realized by using wide bandwidths (up to 4 GHz) in these channels.

To simulate the HATPRO measurements, we use a radiative transfer operator consisting purely of a 1D emission-only forward integration of the radiative transfer equation, which generates brightness temperatures monochromatically at the HATPRO center frequencies. For the calculation of the absorption coefficients, a fast absorption predictor (Löhnert et al. 2004) based on Rosenkranz's (1998) millimeter-wave absorption model is employed to enhance the speed of the Jacobian calculations. In clear-sky situations, this so-called microwave forward model needs profiles of temperature, humidity, and pressure to be able to simulate realistic brightness temperatures; other gaseous atmospheric constituents play only a minor role at the HATPRO center frequencies from the perspective of a ground-based upward-looking instrument. To take into account the estimated random error of real HATPRO measurements, the error numbers listed in Table 1 are randomly added to the forward model simulations. These error estimates include typical radiometric noise, calibration uncertainties, and random uncertainties in the fast absorption predictor.

b. AERI

The AERI is an operational infrared spectrometer that measures the downwelling infrared radiance from 3.3–19 μm (3020–520 cm^{-1}; see Fig. 1) at 1-cm^{-1} resolution (Knuteson et al. 2004a,b). Two detectors are used in a ''sandwich'' configuration to provide the needed sensitivity across the entire spectral range. Details on the calibration approach and accuracy are provided by Knuteson et al. (2004b). The random noise in the AERI observations is determined from the imaginary component of the calibrated radiance (Knuteson et al. 2004b), and thus any scene-dependence of the noise level is automatically captured for each sample. The AERI is typically run in one of two temporal sampling modes: 1) ''normal sample'' mode, whereby sky radiance is averaged for 3 min followed by views of the two calibration blackbodies, resulting in an approximate 7-min temporal resolution; and 2) ''rapid sample'' mode, where sky radiance is averaged for 12 s and multiple (8–10) sky averages are collected before the blackbodies are viewed. Although the rapid-sample data have approximately 4 times more random noise than the normal-sample data, a principal component-based noise filter is used to remove the uncorrelated random error from the AERI observations, which results in a similar noise level in the rapid-sample data as that in the normal-sample data (Turner et al. 2006).

The AERI has approximately 2500 spectral channels for each of its two detectors. Previous studies (e.g., Turner 2005) have assumed that the random noise between any two of these spectral channels is independent. We have confirmed this by analyzing a long time series of observations where a well-characterized blackbody was placed in the sky port. The analysis of these data demonstrated that the absolute value of the correlation coefficient between any two spectral channels was less than approximately 0.3, and there was no apparent pattern identified when the correlation matrix was plotted (not shown).

Like the microwave spectrum, the infrared spectrum also contains information on the vertical profile of temperature and humidity. Smith et al. (1999) and Feltz et al. (1998) used spectral observations from 612–713 and 2223–2260 cm^{-1} (i.e., measurements from the 15- and 4.3-μm CO_2 bands, respectively) for temperature profiling, and observations from 538–588 and 1250–1350 cm^{-1} (i.e., measurements from the wings of the rotational and 6.3-μm water vapor bands, respectively) for water vapor

TABLE 1. Description of microwave (M1, M2) and infrared (A1–A4) bands and the assumed instrumental noise used for the different retrieval setups.

Band M1 center frequency (GHz)/noise (K)	Band M2 center frequency (GHz)/noise (K)	Band A1 range (cm^{-1})	Band A2 range (cm^{-1})	Band A3 range (cm^{-1})	Band A4 range (cm^{-1})
		No. of channels	No. of channels	No. of channels	No. of channels
		Noise (mW m^{-2} sr^{-1} cm)	Noise (mW m^{-2} sr^{-1} cm)	Noise (mW m^{-2} sr^{-1} cm)	Noise (mW m^{-2} sr^{-1} cm)
22.24/0.4	51.26/0.5	538–588	675–713	1250–1350	2223–2260
23.04/0.4	52.28/0.5				
23.84/0.4	53.86/0.5	104	79	208	77
25.44/0.4	54.94/0.2				
26.24/0.4	56.66/0.2	1.8	0.30	0.25	0.011
27.84/0.4	57.30/0.2				
31.40/0.4	58.00/0.2				

profiling. Our analysis demonstrated that the information content on both the longwave side (612–660 cm^{-1}) and shortwave side (675–713 cm^{-1}) of the 15-μm CO_2 band are essentially equivalent, and because the random noise level is higher on the longwave side of the band, we will not include the observations from the 612–660 cm^{-1} band in this study. Thus, our analysis focuses on the four distinct bands A1–A4 of the AERI shown in Table 1.

To simulate the AERI measurements, a fast-transmittance forward model based upon Eyre and Woolf (1988) is utilized. This ''fastaeri'' model treats water vapor and ozone as variable gases, but holds the others fixed to values in the *U.S. Standard Atmosphere, 1976.* The carbon dioxide profile is set to have a constant mixing ratio of 380 ppmv, and the contributions from chlorofluorocarbons (CFCs) are not included in the model. The fastaeri model was constructed using output from the Line-by-Line Radiative Transfer Model (LBLRTM), version 11.3, which includes version 2 of the Mlawer–Tobin–Clough–Kneizys–Davies (MT-CKD) water vapor continuum model (Clough et al. 2005).

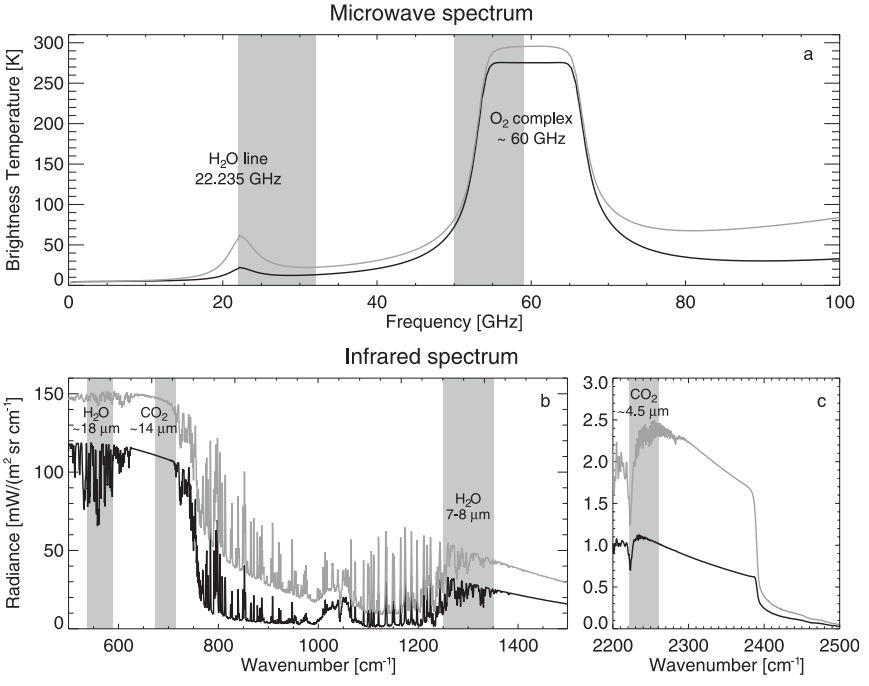

FIG. 1. Areas (gray shaded) of the (a) microwave and (b),(c) infrared spectra used for temperature and humidity profiling in this study. The light gray and black lines depict the spectra during a humid summer day at Payerne (IWV ~ 30 kg m^{-2}) and during a typical winter day with low amounts of water vapor (~8 kg m^{-2}). The associated atmospheric profiles are shown in Fig. 3.

The monochromatic layer-to-surface transmission profiles from the LBLRTM are convolved with the AERI's spectral response function (a sinc function), the effective layer optical depths at each AERI spectral channel are computed by taking ratios of the convolved transmittance profiles at different layers, and these layer optical depths are related to the atmospheric state predictor variables at those layers via linear regression. The fastaeri model contains both uncorrelated error (because each of the regressions for each spectral channel were determined independently of the other channels) and correlated error that comes from inadequacies in the LBLRTM (such as errors in the formulation of the water vapor continuum). The model's uncorrelated error is assumed to be smaller than the uncorrelated error in the normal-sample AERI data. The correlated error in the model would most likely manifest itself as a bias, and we have assumed for this study that the forward models are unbiased estimators; thus, we are assuming that the correlated error in the model is negligible. Note that fastaeri is an emission-only model that does not include scattering (i.e., realistic clouds cannot be simulated). The fastaeri model has been used extensively in previous analyses of water vapor and temperature from the AERI (e.g., Smith et al. 1999; Feltz et al. 2003).

For this sensitivity study, the fastaeri model was used to compute radiance with the spectral resolution of the AERI, and uncorrelated random noise was added to these calculations. We utilized the average noise level of a normal-sampling AERI system in clearsky cases (Knuteson et al. 2004b). This translates into 1-sigma uncertainties of bands A1–A4 given in Table 1.

3. Retrieval methodology

The true atmospheric state vector **x,** which we are retrieving in this study, consists of vertical profiles of atmospheric temperature ($\mathbf{T}$) and absolute humidity ($\boldsymbol{\rho}_v$), such that we can notate $\mathbf{x} = (\mathbf{T}, \boldsymbol{\rho}_v)$. The vertical resolution used in the retrieval algorithm for both temperature and humidity is set to 50 m in the lowest 200 m and then increases gradually to 150 m at 1000 m, 250 m at 3000 m, and 500 m at 10 km above the surface (total of 43 levels), which corresponds approximately to typical height grids used in state-of-the-art NWP models.

a. Measurement inversion

The goal of the applied inversion scheme, the integrated profiling technique (IPT; Löhnert et al. 2004) algorithm, is to retrieve $\mathbf{x}$ by optimally exploiting the information from a given measurement vector $\mathbf{y}$ (Rodgers 2000). Depending on the situation, $\mathbf{y}$ will consist of a vector of observed microwave brightness temperatures and/or infrared radiances. Generally in remote sensing applications, determining $\mathbf{x}$ from $\mathbf{y}$ directly is an underdetermined and ill-conditioned problem, meaning that no unique solution exists and that very small errors in the measurement may lead to huge deviations in the retrieved atmospheric profile. Approaches to increase the number of degrees of freedom of the solution vector are to combine complementary measurements or add a source of a priori information to the retrieval problem, which is the seasonal mean profile in our case. If the relationship between $\mathbf{x}$ and $\mathbf{y}$ is slightly to moderately nonlinear, an optimal atmospheric state $\mathbf{x}_{\text{op}}$ can be found by iterating the following formulation:

$$\mathbf{x}_{i+1} = \mathbf{x}_i + (\mathbf{K}_i^{\mathrm{T}}\mathbf{S}_e^{-1}\mathbf{K}_i + \mathbf{S}_a^{-1})^{-1}[\mathbf{K}_i^{\mathrm{T}}\mathbf{S}_e^{-1}(\mathbf{y} - \mathbf{y}_i) + \mathbf{S}_a^{-1}(\mathbf{x}_a - \mathbf{x}_i)], \quad (1)$$

where i represents the iteration step, $\mathbf{x}_a$ represents the a priori knowledge of $\mathbf{T}$ and $\boldsymbol{\rho}_v$, $\mathbf{S}_a$ represents the a priori covariance matrix, and $\mathbf{S}_e$ represents the combined measurement and forward model error covariance matrix. The Jacobian, or the sensitivity of the forward model to changes in $\mathbf{x}$, is denoted by $\mathbf{K}_i = \partial\mathbf{F}(\mathbf{x}_i)/\partial\mathbf{x}_i = \partial\mathbf{y}_i/\partial\mathbf{x}_i$, where $\mathbf{K}_i$ is recalculated for each iteration using finite differences. The forward model $\mathbf{F}$ transforms from the state space ($\mathbf{x}$) to the measurement space ($\mathbf{y}$) in a straightforward way; that is, given a state space vector at a certain iteration $\mathbf{x}_i$, $\mathbf{F}$ calculates $\mathbf{y}_i$ by applying the radiative transfer operators described in sections 2a and 2b to compute the brightness temperatures and/or radiance at the microwave frequencies and/or the infrared wavenumbers.

Optimally, the formulation of Eq. (1) should guarantee the minimization of a quadratic cost function between $\mathbf{x}_a$ and $\mathbf{x}_i$, and also between $\mathbf{y}$ and $\mathbf{y}_i$, when the difference between $\mathbf{x}_{i+1}$ and $\mathbf{x}_i$ goes toward zero. The iteration procedure is terminated after an optimal number of iterations (i = op) when IPT has converged to a sensible point (i.e., when the change in $\mathbf{x}_i$ is small). This is determined when the cost function reaches an adequate minimum, yielding the solution $\mathbf{x}_{\text{op}}$. Rodgers (2000) describes a method to judge whether the iteration procedure has reached convergence by considering a quadratic cost function between $\mathbf{F}(\mathbf{x}_i)$ and $\mathbf{F}(\mathbf{x}_{i+1})$:

$$[\mathbf{F}(\mathbf{x}_{i+1}) - \mathbf{F}(\mathbf{x}_i)]^{\mathrm{T}}\mathbf{S}_{\delta\mathbf{y}}^{-1}[\mathbf{F}(\mathbf{x}_{i+1}) - \mathbf{F}(\mathbf{x}_i)] \ll d, \quad (2)$$

with d denoting the dimension of $\mathbf{y}$ and $\mathbf{S}_{\boldsymbol{\delta}\mathbf{y}}$ the covariance matrix between the measurement $\mathbf{y}$ and $\mathbf{F}(\mathbf{x}_{\text{op}})$. If this criterion is not fulfilled after 10 iterations, the retrieval is aborted. It is important to note that the solution $\mathbf{x}_{\text{op}}$ must be interpreted as the most probable

solution of a Gaussian distributed probability density function, whose covariance can be written as

$$\mathbf{S}_{\mathrm{op}} = (\mathbf{K}_i^{\mathrm{T}}\mathbf{S}_e^{-1}\mathbf{K}_i + \mathbf{S}_a^{-1})^{-1}. \quad (3)$$

The diagonal elements of this matrix give an estimate of the mean quadratic error of $\mathbf{x}_{\mathrm{op}}$, whereas the off-diagonal elements yield information on the correlation of retrieval errors between the different heights.

A further important measure for retrieval algorithm evaluation is the averaging kernel matrix $\mathbf{A}$ that states the sensitivity of the retrieved to the true state ($=\partial\mathbf{x}_{\mathrm{op}}/\partial\mathbf{x}$). In the case of Gaussian statistics, $\mathbf{A}$ can be written as

$$\mathbf{A} = \mathbf{S}_{\mathrm{op}}(\mathbf{K}_{\mathrm{op}}^{\mathrm{T}}\mathbf{S}_e^{-1}\mathbf{K}_{\mathrm{op}}). \quad (4)$$

The diagonal values of $\mathbf{A}$ are frequently used as a measure of vertical resolution (Rodgers 2000), whereas the trace of $\mathbf{A}$ states the independent number of levels that can be retrieved from a given measurement.

b. A priori information

In this study, our goal is to show the potential of a combined HATPRO–AERI observation system for temperature and humidity retrieval. For this reason we do not use any other a priori information besides a long-term radiosonde climatology. Löhnert et al. (2007) have shown how the microwave profiler retrievals can be enhanced by including additional in situ measurements such as close-by radiosonde ascents. However, this paper's main goal is to assess the accuracy of the temperature and humidity retrievals solely from microwave and infrared measurements alone.

To evaluate the information content from the two instruments relative to each other, we utilize data from two climatically different stations. The first station considered is Payerne, Switzerland, which represents a typical central European climate, located at 46°49′N and 6°97′E at 492 m above sea level. The a priori profiles $\mathbf{x}_a$ were calculated as seasonal means using 9446 radiosonde ascents over a time period from 1992 to 2006. The second station considered is Darwin, Australia, which represents a humid tropical climate, located at 12°42′N and 130°89′E at 30 m above sea level. Here 2218 radiosonde ascents over a time period from 1992 to 2005 passed the quality control procedure and thus were used to determine the a priori profiles. All radiosondes were subject to a sophisticated quality control procedure (Nörenberg et al. 2008) to guarantee the use of only physically realistic ascents. The covariance matrices $\mathbf{S}_a$ were calculated 4 times for each station (i.e., as a function of season), with the variances of $\mathbf{T}$ and $\boldsymbol{\rho}_v$ at each vertical level on the diagonal and the covariances between the different levels in the off-diagonal components. Note that the covariances between $\mathbf{T}$ and $\boldsymbol{\rho}_v$ have also been considered.

c. S_e matrix

For this simulation study, the error covariance matrix $\mathbf{S}_e$ contained only nonzero elements on the diagonal components and the off-diagonal components were set to zero, which assumes that the measurement uncertainties between any pair of wavelengths are uncorrelated. This matrix is used to describe the expected measurement accuracy of the HATPRO and AERI instruments. For the HATPRO simulations, the error numbers were set to the square values of the noise levels listed in Table 1. For the AERI, the square of the 1-sigma uncertainties of bands A1–A4 given in Table 1, which were described in section 2b, were used along the diagonal of the $\mathbf{S}_e$ matrix, and zeros were utilized on the off diagonal.

4. Retrieval evaluation

Only CS radiosonde ascents were used in the retrieval simulation. A simple relative humidity threshold scheme was applied to identify CS cases, where radiosondes were classified as CS when the relative humidity remained below the threshold value of 95% throughout the entire profile. Approximately 70% and 79% of the radiosonde ascents at Payerne and Darwin, respectively, were determined to be CS. This does not necessarily guarantee that the atmosphere was free of condensate during the time of these ascents; however, this is not essential in the retrieval process because clouds are not considered in the forward model. HATPRO brightness temperatures and AERI radiances have been simulated from pressure, temperature, and humidity profiles from a subset of the CS radiosonde ascents equally spanning all seasons: 620 and 643 cases were selected at Payerne and Darwin, respectively. The difference in climatology of these two sites is shown in the distributions of surface temperature and IWV (Fig. 2). The Payerne site shows a much cooler and broader (282.1 ± 7.5 K) distribution of surface temperature in comparison to the Darwin site (300.6 ± 2.2 K), indicating fairly warm and constant low-level temperatures at the latter site. However, Darwin shows a higher standard variation in IWV (12.5 kg m^{-2}) with values peaking around 70 kg m^{-2} and a mean value of 40.2 kg m^{-2} in comparison to a mean value of 14.9 kg m^{-2} and a variation of 7.3 kg m^{-2} at the Payerne site. These two significantly different sites were chosen for retrieval evaluation to test the sensitivities of the MW and IR retrievals under a wide range of conditions.

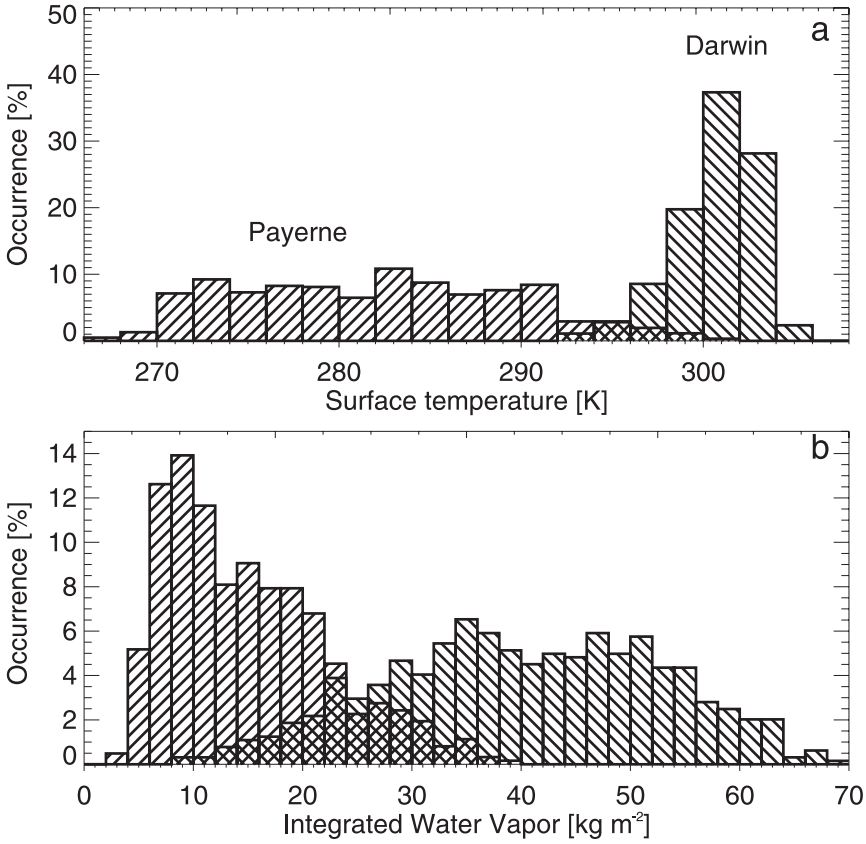

FIG. 2. Distributions of (a) surface temperature and (b) IWV for the Payerne (N= 620 cases) and Darwin (N= 643 cases) sites during selected clear-sky scenes.

We then applied the above described retrieval method to six different setups of the simulated measurement vector **y**. The first four setups encompass two microwave-only and two infrared-only retrieval configurations (see Table 2). The microwave zenith-only (MZ) setup applies only zenith-looking simulations from all the HATPRO channels (bands M1 and M2), whereas the microwave zenith plus elevation retrieval (ME) additionally uses the four most opaque channels of band M2 at five further elevation angles (42°, 30°, 10.2°, 19.2°, and 5.4° above the horizon). The standard AERI retrieval setup (AE) uses simulated measurements between 538 and 588 cm^{-1} (band A1) and 1250 and 1350 cm^{-1} (band A3) for water vapor profile information and additionally one side of the 15-μm CO_2 band from 674 to 713 cm^{-1} (band A2) for temperature profiling. The second AERI (AE4) retrieval setup uses the standard AERI setup plus the channels from 2223 to 2260 cm^{-1} (band A4). The remaining two retrieval configurations then constitute the combinations of MZ and AE (MZAE) and MZ and AE4 (MZAE4) for joint retrieval evaluation.

a. Retrieval example

Two spectra (Fig. 1), which represent typical dry and moist cases, were used as input into the MW and IR retrieval algorithms (Fig. 3). In the moist summer case, both the MZ and the AE retrieval show very similar results in matching the almost-dry-adiabatic lapse rate in the lower troposphere. The spectral information content in both microwave and infrared data is too low to resolve the lifted inversion around 4 km, as the weighting functions for these ground-based sensors become quite broad in the mid–upper troposphere. For this reason, we have restricted our analysis to heights below 5 km. The temperature retrieval for the drier winter case clearly shows that the AE retrieval is able to reproduce the strong lifted inversion at ~1 km more accurately than the MZ retrieval, which shows clear ''smoothing'' effects. This also holds true for both summer and wintertime humidity profile retrievals. The AE retrieval shows potential to retrieve distinct features of the humidity profiles, such as the fairly constant $\boldsymbol{\rho}_v$ values in the BL and the following abrupt decrease with height in the winter case, as well as the humidity increase around 2 km in the summer case.

TABLE 2. Description of different measurement configurations and their overall retrieval performance averaged over 0–5 km.

Name	Measurements used	Successful convergence (%) (Payerne/Darwin)	Temperature retrieval accuracy (K): mean RMSE 0–5 km (Payerne/Darwin)	Humidity retrieval accuracy (g m^{-3}): mean RMSE 0–5 km (Payerne/Darwin)
MZ	Bands M1, M2	88/99	1.22/0.86	0.66/1.24
ME	Bands M1, M2 (elevation scanning in band M2)	90/98	0.95/0.73	0.65/1.19
AE	Bands A1, A2, A3	71/84	0.69/0.71	0.42/1.15
AE4	Bands A1, A2, A3, A4	70/87	0.64/0.65	0.41/1.05
MZAE	Bands M1, M2, A1, A2, A3	74/83	0.67/0.67	0.41/0.99
MZAE4	Bands M1, M2, A1, A2, A3, A4	72/85	0.64/0.62	0.38/0.94

Additionally, the diagonal components of $\mathbf{S}_{op}$ have been evaluated for retrieval error characterization (Fig. 4). As expected from Fig. 3, the error in the AE retrieval for $\mathbf{T}$ and $\boldsymbol{\rho}_v$ is smaller than the error in MZ, both in the winter and summer cases. Note that for the winter case, the $\boldsymbol{\rho}_v$ accuracy of AE is better than of MZ by almost a factor of 4. To test the sensitivity of the assumed magnitude of the instrument random noise, the HATPRO and AERI noise levels have been multiplied by 0.5 and 2 and the retrieval was then reapplied (Fig. 4). For these two example profiles, the sensitivity of the MZ retrieval to changes in the assumed magnitude of the random error in the instrument is significantly smaller than for the AE retrieval, with the changes in MZ retrieval accuracy ranging from 8% to 18% and the changes in the AE retrieval accuracy ranging from 40% to 100%. The instrument noise level has relatively little influence on the MZ retrieval accuracy of $\boldsymbol{\rho}_v$ above 1.2 km (winter) and 2.5 km (summer). This suggests that the MW measurements add no significant amount of information to retrieval accuracy above these heights. However, the retrieval will still perform more accurately than the assumption of the seasonal a priori profile resulting from the level-to-level correlation contained in $\mathbf{S}_a$. The much higher sensitivity of AE to the assumed instrumental noise reflects the fact that there is generally more information contained in the AERI compared to the HATPRO measurements. If the error noise assumptions for the AERI (Table 1) are too conservative and/or are significantly reduced by principal component analysis noise filter (section 2b), then AE retrievals may be much more accurate than assumed; however, if the uncertainties in the AERI observations are larger than expected, MZ may even outperform AE—especially in high-humidity cases above the lower BL.

b. Statistical retrieval evaluation

We applied the retrieval technique to the six different configurations of the simulated measurement vector $\mathbf{y}$ (Table 2) for the selected CS scenes at each site. Figures 5–8 show the derived accuracies from the retrieval simulations as a function of height above ground. Each

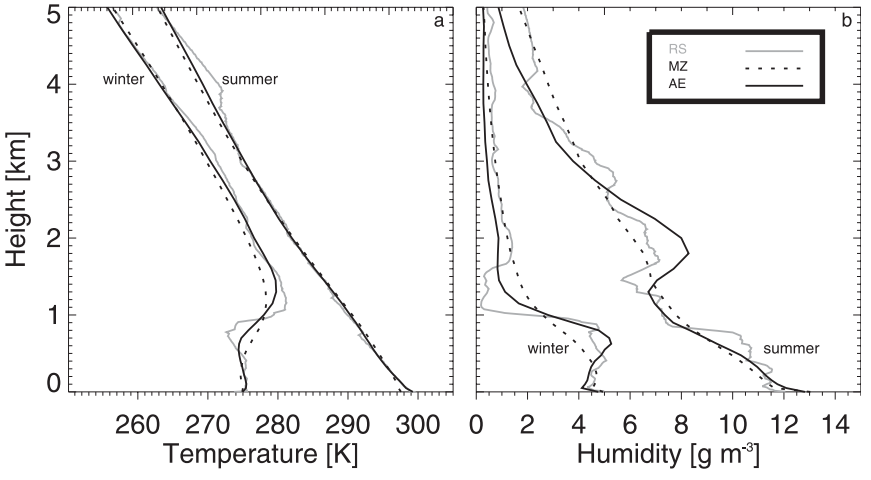

FIG. 3. Profiles of (a) temperature and (b) humidity for a summer and winter case at Payerne. Shown are radiosonde measurements (gray), MZ retrievals (dotted), and AERI retrievals without the 4-μm channel (AE; solid).

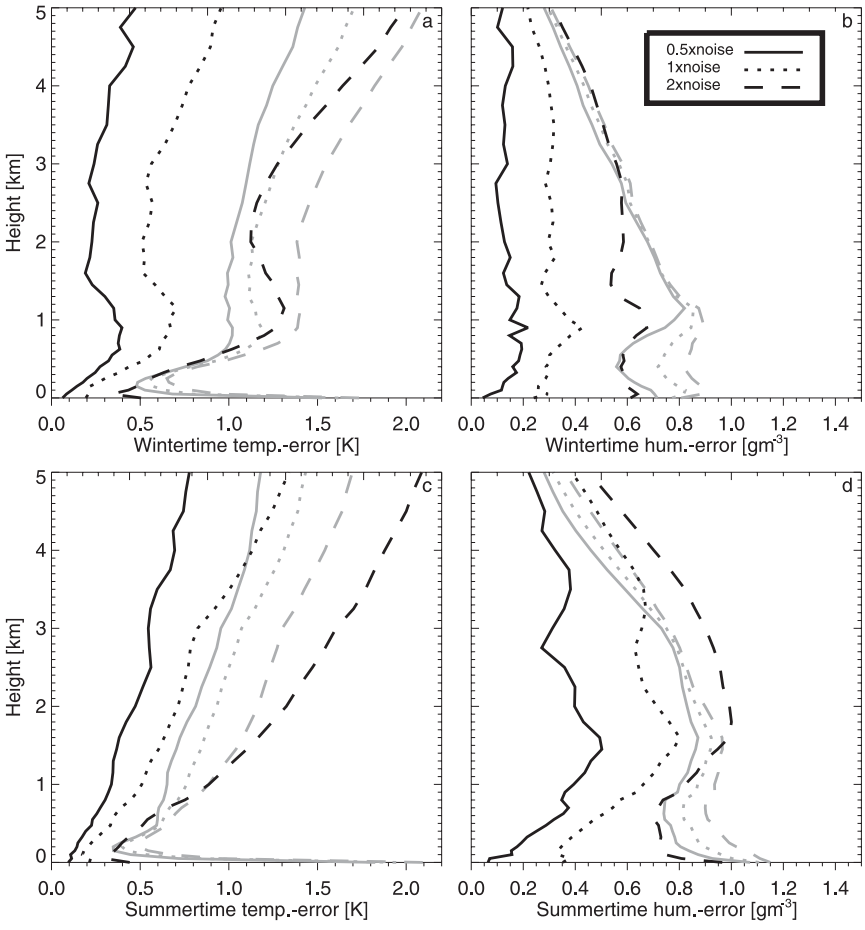

FIG. 4. (left) Temperature and (right) humidity accuracies (square root of the diagonal values of $\mathbf{S}_{op}$) for the (top) wintertime and (bottom) summertime cases shown in Fig. 3 as a function of assumed instrumental random noise. Noise as given in Table 1 (dotted line), noise values multiplied by 0.5 (solid), and noise values multiplied by 2 (dashed). Black lines indicate results from AE retrieval; gray lines indicate results from MZ retrieval.

of these figures only shows an analysis of those cases where all of the shown methods converged simultaneously. Because of this, the number of cases shown in each figure may vary but is noted in each figure caption. The overall successful convergence rate for each retrieval configuration is also shown in Table 2. Generally the microwave-only retrieval success rates are higher than those configurations that include AERI data. Typically, the AERI retrievals need more iterations and if the first guess (here the a priori profile) is too far from the ''true'' atmospheric state, an adequate solution [Eq. (2)] is often not found after 10 iterations. In these cases, the algorithm often tends toward nonphysical parameters (e.g., unrealistically high supersaturation). The higher success rate in Darwin, relative to the Payerne site, can be explained by the very small variability of the temperature profile. Thus, the temperature profile is described by the a priori profile to a higher degree, which helps the retrieval find a minimum more effectively and faster.

1) PAYERNE

The performance of the different single-instrument retrievals (Fig. 5) show similar temperature RMSE accuracies in the lowest 500 m for ME, AE, and AE4 ranging from 0.2 to 0.5 K. These low error values are very suitable for lower BL profiling and underline that HATPRO in elevation-scanning mode is able to perform similarly to the AERI in this range. At higher altitudes the ME accuracies more closely resemble those of MZ, which performs poorest throughout the lowest 5 km. MZ accuracies are rather poor at the surface (~2.0 K RMS), decrease to 0.5 K in the lower boundary layer, and increase back to ~2 K at 5 km. The high values at the surface are due to the comparably high variability of the temperature resulting from local influences of the

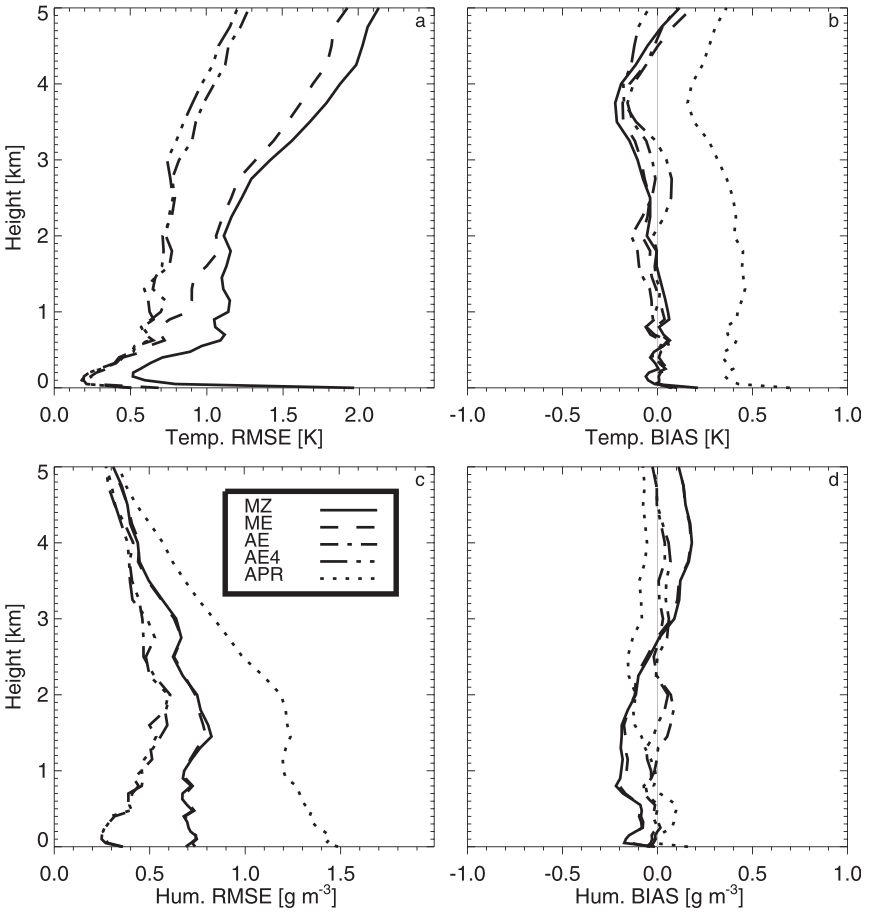

FIG. 5. (top) Temperature and (bottom) humidity (left) RMSE and (right) bias error for the retrievals applied to the Payerne dataset computed from $N = 304$ successful and simultaneous MZ retrievals (solid lines), ME retrievals (dashed), AE retrievals (dot–dashed), and AERI retrievals with the 4-μm channels (AE4; dot–dot–dot–dashed). The error characteristics of the a priori profiles (mean seasonal climatology) are also shown (dotted). Note that the a priori RMSE of temperature is in the range of 4–5 K and thus is not shown here.

turbulent energy fluxes. This variability is not captured by MZ, because the zenith-pointing microwave measurements can only represent the temperature of a ~30–40-m-thick layer above the ground. By measuring at low elevation angles, ME is able to capture this variability. Both AE and AE4 accuracies, on the contrary, remain below 1 K up to 4-km height. AE and AE4 accuracies are very similar showing that the use of the shoulder of the 4-μm CO_2 absorption band does not significantly enhance the accuracy of the temperature retrieval and thus is not needed. Furthermore, this study has not accounted for the possible solar scattering contribution to the 4-μm signal that may result from an aerosol-loaded sky, which would further impact the accuracy of the retrieval in the AE4 configuration.

The accuracies of the humidity retrieval in the BL show significant differences between HATPRO and AERI. The AE accuracies are as low as 0.25 g m^{-3} in the lower BL, slowly increasing to 0.6 g m^{-3} at 2 km, whereas the MZ retrieval shows constant values around 0.75 g m^{-3} in the same height range. Thus, as also indicated in the example profiles in Fig. 3, the AERI retrievals show the ability to resolve more vertical humidity structure than the HATPRO retrievals. However, both AERI and HATPRO retrievals are still significantly more accurate than the mean seasonal climatology (which is indicated by the a priori profiles as dotted lines). For temperature and humidity retrievals, the bias errors are rather small relative to the RMSE. Of all humidity retrievals, MZ and ME exhibit the largest bias errors in the range of -0.15 g m^{-3} in the lower 2.5 km and $+0.15$ g m^{-3} in the upper 2.5 km, whereas the biases from AE and AE4 retrievals are insignificant. The bias in the a priori data shown in

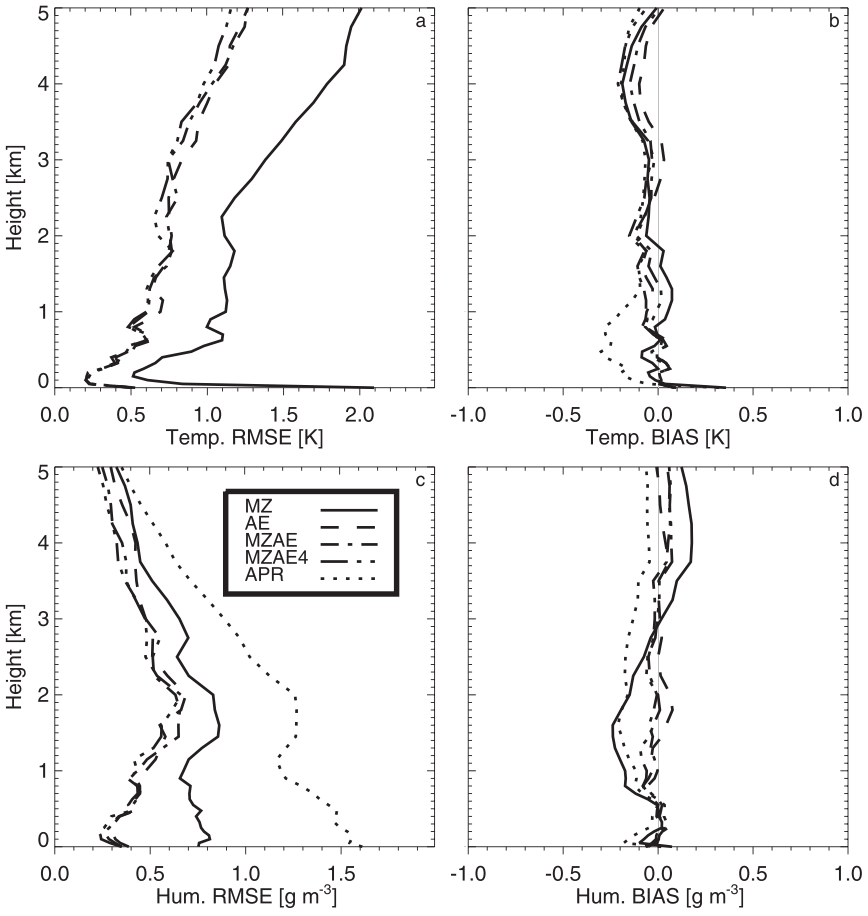

FIG. 6. As in Fig. 5 but from $N = 272$ successful and simultaneous MZ (solid), AE (dashed), MZAE (dot–dashed), and MZAE4 (dot–dot–dot–dashed) retrievals.

Fig. 5 is a result of regarding only a subsample of the original data from which the mean seasonal profiles were derived (i.e., the subset of cases that converged for all four retrieval methods). Figure 5b nicely shows that this ''seasonal bias'' is corrected for by all retrievals; however, certain artifacts such as the curvature between 3 and 4 km (Fig. 5b) are maintained. This is a result of the statistical correlation between each of the levels, which is prescribed in the $\mathbf{S}_a$ matrix.

The combination of both MZ and AE or MZ and AE4 into one physical retrieval scheme shows no significant improvement in the retrieved temperature and humidity profiles compared to the AE retrieval alone in the Payerne dataset (Fig. 6). The behavior of the combined retrievals—both from the RMSE and bias error point of view—is very similar to that of AE. This clearly demonstrates that no significant additional information is added from the microwave profiler measurement to the spectral infrared measurements. This conclusion, however, is only strictly valid for an atmosphere containing no clouds and no significant amount of aerosol.

In the current retrieval configuration, the computation of the Jacobian matrix $\mathbf{K}_i$ requires a perturbation of 43 temperature and humidity values at each iteration step. Mainly because of the computing time for the forward calculations with the fastaeri model, this requires a significant amount of time for an AE profile to converge (~180 s on a standard Linux PC as compared with ~15 s for the MZ retrieval). Because future applications of this retrieval technique will include the retrieval of clouds and aerosol (and thus the inclusion of even more time-consuming scattering calculations), it is highly desirable to significantly reduce this calculation time without losing too much accuracy. To achieve this goal, empirical orthogonal functions (EOFs) have been separately derived for the temperature and humidity profile at each site. Analysis of the EOF data reduction using the objective algorithm by Turner et al. (2006) showed that both temperature and humidity profiles at Payerne can be sufficiently described by 10–15 EOFs (eigenvectors). In this case, the state vector $\mathbf{x}$ consists only of the EOF coefficients. These coefficients are

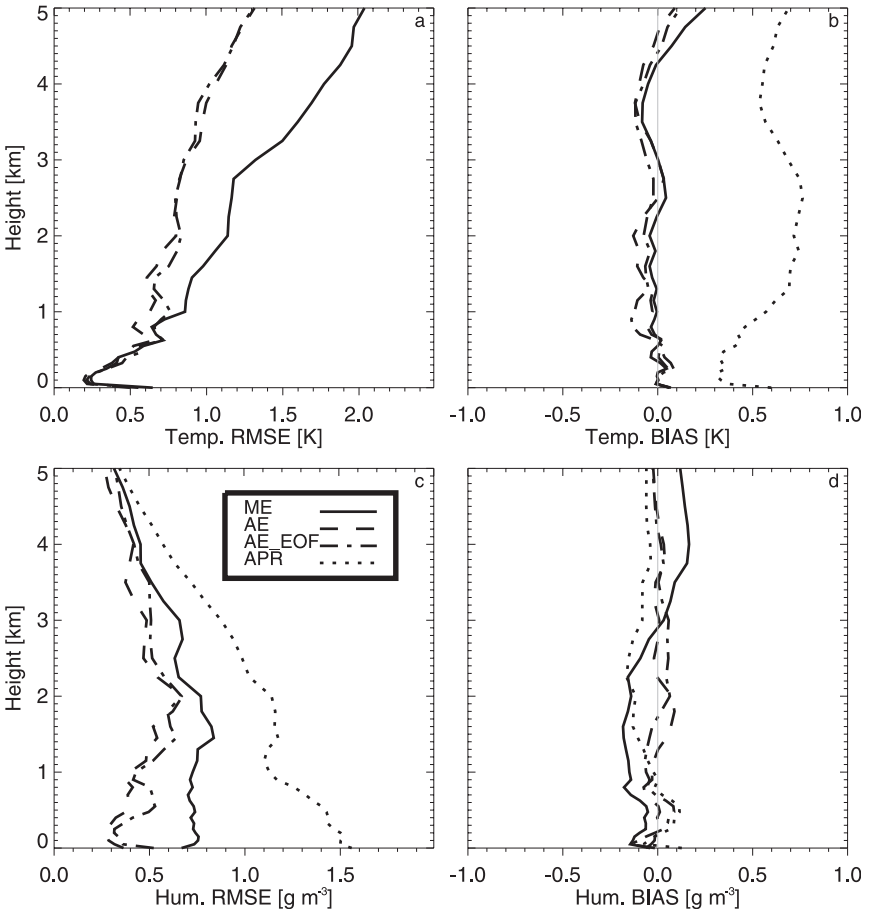

FIG. 7. As in Fig. 5, but from $N = 276$ successful and simultaneous MZ retrievals (solid lines), AE retrievals (dashed), and AERI retrievals derived with an EOF decomposition for temperature and humidity using 10 separate eigenvectors for each variable (AE_EOF; dash–dotted).

multiplied with the corresponding eigenvector and subsequently summed up to obtain the profile. The finite-difference calculations to compute **K** are thus performed in a space with smaller dimensionality, allowing **K** to be computed much more efficiently. However, before calling the forward model, the perturbed EOF-coefficient vector is transformed back into state space. Retrieving temperature and humidity profiles in EOF space for AE (AE_EOF) and subsequently transforming back into state space shows essentially no loss of accuracy in the retrieved temperature profile (Figs. 7a,b). An exception may be the height range 800–1200 m where inversions at the top of the boundary layer frequently occur. The RMSE accuracy of the retrieved humidity profile (Fig. 7c) is also only partially reduced in the lower 2 km, with maximum RMSE increases on the order of 0.15 g m^{-3}. The humidity bias error characteristics are not affected (Fig. 7d). The advantage of the EOF decomposition is that computation time for a successful retrieval is reduced by a factor of 3–4, provided that the above-mentioned decrease in accuracy is acceptable.

2) DARWIN

In the much warmer and moister tropical climate, the retrieval behavior (Fig. 8) does differ significantly to the central European climate (Fig. 5). RMSE values for all temperature retrievals in the lowest 500 m are lower at the Darwin site because of the less pronounced diurnal cycle in the tropics. Here, the lapse rate is frequently close to adiabatic, whereas typical nighttime inversions and daytime adiabatic lapse rates in central Europe result in higher temperature variability of the BL. Fewer temperature inversions, which are difficult to capture with any retrieval algorithm, occur in the tropical climate. Above 1-km height, the addition of the microwave channels (i.e., MZAE) or the 4-μm channel to the AE retrieval (AE4) results in a slight accuracy improvement of ~0.1 K (Fig. 8a). However, above 3 km,

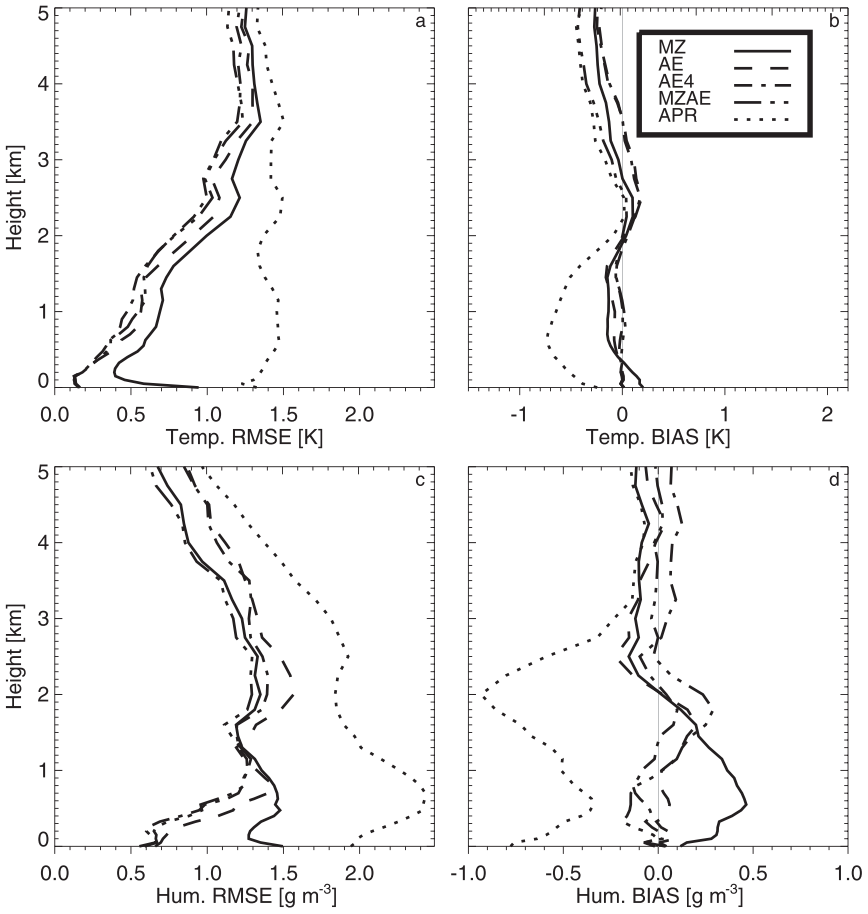

FIG. 8. As in Fig. 5 but applied to the Darwin dataset computed from $N = 459$ successful and simultaneous MZ (solid), AE (dashed), AE4 (dot–dashed), and MZAE (dot–dot–dot–dashed) retrievals.

all RMSE curves slowly evolve toward the a priori RMSE curve indicating no benefit to retrieval at these heights.

In the case of humidity RMSE values at the tropical site, AE is only superior to MZ up to a height of ~1 km (Fig. 8c). Above this height, the large amounts of water vapor in the tropics result in a more opaque atmosphere for the AERI, so that the vertical resolution at higher altitudes diminishes. The water vapor absorption is much weaker for the microwave channels employed here, making the atmosphere much more transparent; thus, the MZ retrieval suffers no loss of sensitivity as the IWV increases. Additional spectral channels that correspond to weaker water vapor absorption lines (such as in the region from 1200 to 1250 cm^{-1}) could be included in the AERI's observational vector, which would improve the AERI retrievals in these moist environments; however, we have not pursued this here to keep the parameters for the retrieval as consistent as possible between Payerne and Darwin. As a consequence, the MZAE combination shows the best RMSE results throughout the profile. Generally, the RMSE humidity accuracies are poorer for the Darwin site than for the Payerne site, but the absolute values and the variability are higher at Darwin also.

The a priori bias of both temperature and humidity for the chosen tropical dataset are higher than in the central European case. For the temperature retrievals at Darwin (Fig. 8c), MZ shows the highest sensitivity to bias error (same as for the Payerne site), whereas the AERI retrievals are less sensitive and can compensate for the a priori bias in the lowest 2 km. Above this height, the bias error of all retrievals follows the curvature of the a priori bias, with an overall reduction of bias error. In the case of the humidity retrieval, the a priori bias of the data subset is too large to be entirely compensated by any of the retrieval configurations, although the retrievals, including the AERI data, show less sensitivity to the a priori bias in the lowest 1.5 km (Fig. 8d). This result clearly shows that an a priori bias of this magnitude should be avoided. A possible solution to this problem would be to scale the a priori profile

of humidity with a realistic and independent IWV value (e.g., obtainable from a temporally and spatially nearby radiosonde measurement or a GPS measurement).

The main results discussed above are summarized in Table 2, where the RMSE have been averaged over the 0–5-km altitude range to show the benefits and drawbacks of each retrieval configuration that were evaluated. This table demonstrates that the AERI offers significantly more value relative to the HATPRO observations in clear-sky conditions for temperature and humidity profiling, except in very humid conditions.

c. *Degrees of freedom*

An objective way to analyze the information content of the different retrievals is to evaluate the distribution of the number of degrees of freedom of the each single retrieval [Eq. (4); i.e., the number of independent levels of temperature or humidity that can be determined]. For temperature, the distributions of degrees of freedom of MZ and AE do not overlap, neither for the Payerne nor for the Darwin site retrieval simulations (Figs. 9a,c). This clearly demonstrates that AE provides more information on the temperature profile than MZ: on average 5.6 as opposed to 2.4 independent layers. Figure 9a also illustrates that the inclusion of the elevation-scanning mode for the HATPRO can double the amount of independently retrieved levels, but as seen from Fig. 5, this improvement is mostly limited to the lowest 500 m. As expected, ME and MZ do not differ with respect to the humidity retrievals because no additional information about the humidity profile has been added and scanning has only been considered for the channels between 50.8 and 60 GHz, which are sensitive primarily to temperature. For the Darwin site simulations, in comparison with Payerne, the average number of independent levels in the humidity retrievals is reduced for AE (from 6.3 to 4.2) and increased for MZ (from 1.6 to 2.7). For MZ, the increased opacity at the band M1 microwave channels leads to a slightly improved height resolution, whereas the AERI channels in bands A1 and A3 are becoming more opaque and thus resolve the height profile in a less accurate way in the moist tropical environment.

The potential of an instrument to retrieve the temperature or humidity profile with a certain accuracy and vertical resolution depends on the number of independent pieces of information contained in the measurement. The number of independent pieces of information depends to some degree on the number of spectral channels of the observations, the noise levels, and the spectral location of the channels, but it also depends strongly on the spectral characteristics of the absorption lines observed. For example, the oxygen absorption feature from 51 to 60 GHz really comprises 33 different absorption lines, yet it is perceived as one continuous feature (see Fig. 1) because of pressure broadening of the lines. All measurements made along this absorption feature are highly correlated and thus the number of independent pieces of information about the temperature profile is rather low. In the infrared region between 675 and 713 cm^{-1}, the CO_2 absorption lines can be resolved by the instrument (because they do not overlap as much) and there are more distinctly independent spectral features, thereby providing more pieces of information allowing the temperature profile to be better resolved.

5. Conclusions and outlook

We have presented simulation results from two independent ground-based remote sensing instruments, a standard microwave profiler (HATPRO) and an infrared spectrometer (AERI), for lower-tropospheric profiling of temperature and humidity in ''pristine'' clear-sky conditions. To compare both methods objectively, all measurements have been simulated realistically and consistently, and the same optimal estimation retrieval framework was applied to both using the same a priori information. In all cases, the infrared retrievals of temperature and humidity outperform the microwave retrievals concerning RMSE and bias error, although the microwave temperature retrievals that incorporate elevation scans are as accurate as the infrared retrievals in the lowest 500 m. The AERI retrievals show high potential, especially for retrieving humidity in the BL, where accuracies are better than 0.5 g m^{-3} for a central European climate. Distinct differences occur between a tropical and central European climate, where the inclusion of microwave measurements to the spectral infrared measurements within a unified physical retrieval scheme results in a slight improvement because of the higher opacity of the very moist atmosphere in the tropics.

The limited number of sondes (constituting the CS data subset) employed in this study present a trade-off between representativeness and calculation time. However, we believe that the presented statistics reflect the true distribution because the CS data subset was equally distributed over all seasons.

If the error statistics presented here were to be interpreted for climatological studies, a detailed error analysis for the full set of encountered conditions—including cloudy conditions—would be necessary. This is of particular relevance because ~30% of the cases from the entire Payerne dataset show that the relative humidity threshold of 95% was exceeded and thus the presence of clouds in the moist layers was likely. Also, aerosols can

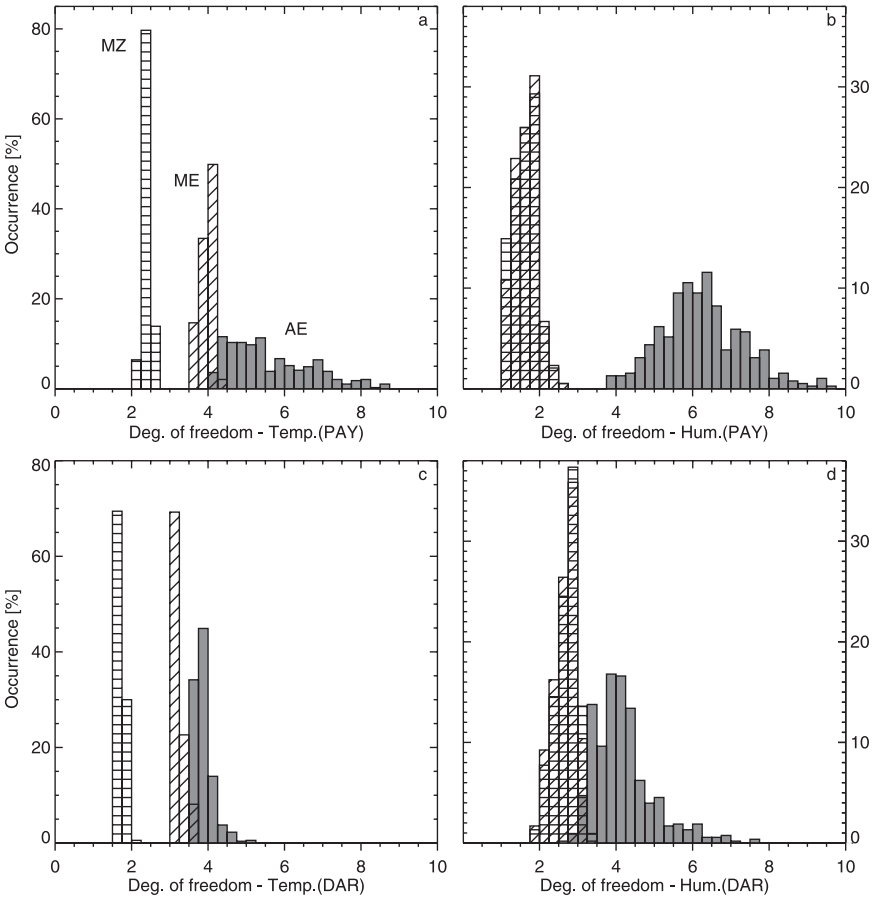

FIG. 9. Histograms of the number of degrees of freedom for (left) temperature and (right) humidity retrievals at the (top) Payerne and (bottom) Darwin sites. The different shading indicates the MZ (horizontal lines), ME (slant lines), and AE (gray shaded) retrievals.

significantly enhance the observed downwelling infrared radiance signal, depending on the aerosol size distribution, optical depth, and composition (e.g., Turner 2008). The simulations presented above have not included aerosol, which will pose an issue when applying the retrieval schemes to real measurements. For a clear-sky retrieval to be successful, an objective classification scheme must be available to rule out the presence of clouds and aerosol, or the radiance contribution from the aerosol and/or cloud layer must be incorporated into the retrieval (either as a priori information or retrieved simultaneously). Note that even very small amounts of column-integrated liquid water content ($\sim$1 g m^{-2}) can lead to nonnegligible signals in an AERI measurement (Turner 2007). Before the application of a clear-sky retrieval, if it cannot be ruled out that clouds or aerosols (especially hydroscopic aerosols leading to cloud formation) are present, a microwave-only retrieval may turn out to be more accurate, because passive microwave measurements are insensitive to aerosol and optically thin clouds.

In this sense, the present study is to be regarded as a starting point for the development toward a joint thermodynamic and cloud, aerosol, and trace gas (e.g., CO, CH_4) retrieval scheme including microwave and infrared measurements; however, appropriate forward models must be employed that have the capability of dealing with multiple gaseous constituents and scattering. The simultaneous use of microwave and AERI observations to retrieve only cloud properties has already been demonstrated by Turner (2007) and Turner and Eloranta (2008). We are currently setting up and testing a sophisticated retrieval scheme for temperature, humidity, cloud phase discrimination, cloud optical depth, and cloud effective radius from simultaneous AERI and HATPRO measurements. In contrast to the results shown here, we expect significant improvements in the retrieved atmospheric state by the HATPRO–AERI combination because clouds are semitransparent in the microwave region. In case of an optically thick cloud in the infrared, which occurs when the liquid water path is

above approximately 60 g m^{-2}, the AERI measurements will yield accurate information on temperature and humidity profiles below the cloud and the cloud-base temperature, as well as—to a certain extent—cloud optical depth, whereas the microwave measurements will give information on temperature and humidity throughout and above the cloud, in addition to the total liquid water content. In the case of an optically thin cloud, the AERI will provide information on cloud effective radius and optical depth and the atmospheric state profiles below the cloud, whereas again the microwave radiometer will provide a reliable source on temperature and humidity profile throughout the troposphere.

Acknowledgments. This work has been supported in part by the U.S. Department of Energy, Office of Science, Office of Biological and Environmental Research, Environmental Sciences division as part of the Atmospheric Radiation Measurement (ARM) Program under Grant DE-FG02-06ER64167. We acknowledge the Payerne Aerological Station of MeteoSwiss and the Australian Bureau of Meteorology for supplying us with the radiosonde data. In addition, the authors thank Dr. Robert Knuteson for his valuable comments and suggestions for improvement of the manuscript.

REFERENCES

Cady-Pereira, K. E., M. W. Shephard, D. D. Turner, E. J. Mlawer, S. A. Clough, and T. J. Wagner, 2008: Improved daytime column-integrated precipitable water vapor from Vaisala radiosonde humidity sensors. *J. Atmos. Oceanic Technol.,* **25,** 873–883.

Clough, S. A., M. W. Shephard, E. J. Mlawer, J. S. Delamere, M. J. Iacono, K. Cady-Pereira, S. Boukabara, and P. D. Brown, 2005: Atmospheric radiative transfer modeling: A summary of the AER codes. *J. Quant. Spectrosc. Radiat. Transfer,* **91,** 233–244.

Crewell, S., and U. Löhnert, 2007: Accuracy of boundary layer temperature profiles retrieved with multifrequency multiangle microwave radiometry. *IEEE Trans. Geosci. Remote Sens.,* **45,** 2195–2201.

Eyre, J. R., and H. M. Woolf, 1988: Transmittance of atmospheric gases in the microwave region: A fast model. *Appl. Opt.,* **27,** 3244–3249.

Feltz, W. F., W. L. Smith, R. O. Knuteson, H. E. Revercomb, and H. B. Howell, 1998: Meteorological applications of temperature and water vapor retrievals from the ground-based Atmospheric Emitted Radiance Interferometer (AERI). *J. Appl. Meteor.,* **37,** 857–875.

——, ——, H. B. Howell, R. O. Knuteson, H. Woolf, and H. E. Revercomb, 2003: Near-continuous profiling of temperature, moisture, and atmospheric stability using the Atmospheric Emitted Radiance Interferometer (AERI). *J. Appl. Meteor.,* **42,** 857–875.

Hewison, T. J., 2007: 1D-VAR retrieval of temperature and humidity profiles from a ground-based microwave radiometer. *IEEE Trans. Geosci. Remote Sens.,* **45,** 2163–2168, doi:10.1109/TGRS.2007.898091.

Knuteson, R. O., and Coauthors, 2004a: Atmospheric Emitted Radiance Interferometer. Part I: Instrument design. *J. Atmos. Oceanic Technol.,* **21,** 1763–1776.

——, and Coauthors, 2004b: Atmospheric Emitted Radiance Interferometer. Part II: Instrument performance. *J. Atmos. Oceanic Technol.,* **21,** 1777–1789.

Löhnert, U., S. Crewell, and C. Simmer, 2004: An integrated approach toward retrieving physically consistent profiles of temperature, humidity, and cloud liquid water. *J. Appl. Meteor.,* **43,** 1295–1307.

——, E. van Meijgaard, H. K. Baltink, S. Groß, and R. Boers, 2007: Accuracy assessment of an integrated profiling technique for operationally deriving profiles of temperature, humidity, and cloud liquid water. *J. Geophys. Res.,* **112,** D04205, doi:10.1029/2006JD007379.

——, S. Crewell, O. Krasnov, E. O'Connor, and H. Russchenberg, 2008: Advances in continuously profiling the thermodynamic state of the boundary layer: Integration of measurements and methods. *J. Atmos. Oceanic Technol.,* **25,** 1251–1266.

Nörenberg, D., S. Crewell, U. Löhnert, and T. Rose, 2008: Development of ground equipment for atmospheric propagation conditions assessment from 10 up to 90 GHz frequency bands (ATPROP). ESA Final Rep. Contract 19839/06/NL/GLC. [Available from ESA-ESTEC, Keplerlaan 1, Postbus 299, 2200 AG Noordwijk, Netherlands.]

Rodgers, C. D., 2000: *Inverse Methods for Atmospheric Sounding: Theory and Practice*. World Scientific, 238 pp.

Rose, T., S. Crewell, U. Löhnert, and C. Simmer, 2005: A network suitable microwave radiometer for operational monitoring of the cloudy atmosphere. *Atmos. Res.,* **75,** 183–200, doi:10.1016/j.atmosres.2004.12.005.

Rosenkranz, P. W., 1998: Water vapor microwave continuum absorption: A comparison of measurements and models. *Radio Sci.,* **33,** 919–928.

Smith, W. L., W. F. Feltz, R. O. Knuteson, H. E. Revercomb, H. M. Woolf, and H. B. Howell, 1999: The retrieval of planetary boundary layer structure using ground-based infrared spectral radiance measurements. *J. Atmos. Oceanic Technol.,* **16,** 323–333.

Turner, D. D., 2005: Arctic mixed-phase cloud properties from AERI lidar observations: Algorithm and results from SHEBA. *J. Appl. Meteor.,* **44,** 427–444.

——, 2007: Improved ground-based liquid water path retrievals using a combined infrared and microwave approach. *J. Geophys. Res.,* **112,** D15204, doi:10.1029/2007JD008530.

——, 2008: Ground-based infrared retrievals of optical depth, effective radius, and composition of airborne mineral dust above the Sahel. *J. Geophys. Res.,* **113,** D00E03, doi:10.1029/2008JD010054.

——, and E. W. Eloranta, 2008: Validating mixed-phase cloud optical depth retrieved from infrared observations with high spectral resolution lidar. *IEEE Geosci. Remote Sens. Lett.,* **5,** 285–288, doi:10.1109/LGRS.2008.915940.

——, B. M. Lesht, S. A. Clough, J. C. Liljegren, H. E. Revercomb, and D. C. Tobin, 2003: Dry bias and variability in Vaisala radiosondes: The ARM experience. *J. Atmos. Oceanic Technol.,* **20,** 117–132.

——, R. O. Knuteson, H. E. Revercomb, C. Lo, and R. G. Dedecker, 2006: Noise reduction of Atmospheric Emitted Radiance Interferometer (AERI) observations using principal component analysis. *J. Atmos. Oceanic Technol.,* **23,** 1223–1238.

Wulfmeyer, V., and Coauthors, 2008: The Convective and Orographically Induced Precipitation Study: A research and development project of the World Weather Research Program for improving quantitative precipitation forecasting in low-mountain regions. *Bull. Amer. Meteor. Soc.,* **89,** 1477–1486.